An innovative method to observe RFQ vanes motion with full-scale RF power and water cooling

Alain C. France, Robin Ferdinand, Olivier Piquet (CEA Saclay, F91191 Gif-sur-Yvette, France)

Abstract The design of high current RFQ's is heavily strained by thermo-mechanical considerations, which eventually have an impact on machining costs, cooling systems, etc. A 1-meter long copper prototype of the SPIRAL2 RFQ has been specifically built to corroborate design options. An innovative method has been developed, allowing real-time observation of mechanical deformations of RFQ vanes, with full-scale RF power and water cooling. Digital images are acquired by a CCD camera, and processed by a dedicated software. Processing includes contrast stretching, low-pass filtering, and block-correlation followed by interpolation. Sub-pixel relative motions of RFQ electrode ends are clearly detected and measured, with RMS errors in the range 0.6 to 1.8 micron.

INTRODUCTION

The SPIRAL2 RFQ prototype (length 1 m, inner diameter 702.4 mm) has been designed to operate at 88 MHz with 40 kW full-power. RFQ copper tube and electrodes are cooled by independent water circuits, and thermo-mechanical simulations have shown that a proper selection of circuit temperatures are required to leave the geometry of axial region (vane tips) unchanged when full RF power is applied, thus saving RFQ room-temperature tuning. One main objective of prototype experiments was to measure the deformations of axial region vs. temperatures and RF power [1]. Variations of a few microns to a few tens of microns were expected.

PROPOSED METHOD

The proposed non-intrusive method consists in acquiring images of the RFQ vanes ends with a CCD camera, and using digital processing to detect motion between each "current" frame and some "reference" frame. Since only deformations are sought, no attempt has been made to relate camera axes to RFQ axes: the four vane ends just need to be present in each camera frame. Vanes are terminated by flat surfaces, which are lit and observed under nearly normal incidence. Rounded edges make precise detection of edge position almost impossible. Using surface texture to detect motion is also difficult, because polished copper is highly reflective. However some artificial etching (here a hand-made grid pattern) can satisfactorily enhance contrast.

Three main categories of algorithms may be used for motion detection. All have to address the fact that CCD cameras deliver *digitized* images (RGB intensities vs. pixel row and column indices), whilst *continuous* motion is to be detected. In group I, intensity f vs. position M and motion Δ are approximated up to 2nd order

$$f(M+\Delta) = f(M) + J^T\Delta + \tfrac{1}{2}\Delta^T H \Delta ,$$

the Jacobian J and Hessian H being estimated from pixel intensities by finite differences. Hessian is used to select plane and tilted intensity facets, and Jacobian to detect X and Y motions of facets. These methods are able to detect largely sub-pixel motions, but require complicated iterative algorithms [2] in case of multi-pixel motion. In group II, digital normalized cross-correlation of "reference" and "current" image is calculated, followed by an interpolator to estimate precise peak position, i.e. X and Y motions. These methods are sensitive and robust; frame may be partitioned in several blocks to eliminate false correlation peaks and derive accuracy [3]. Algorithms based on phase tilt of 2D Fourier transforms [4] are to be placed in the same group (position - spatial frequency duality). In group III, edge detection algorithms are used to extract texture features [5], and pattern recognition yields X and Y motions, rotation and magnification.

A method of group I has been successfully programmed, tested, and finally abandoned, because experiments showed multi-pixel motions. Group III has been explored, but pattern recognition turned out to be quite complicated because many surface defects survive to edge detection. Finally, the correlator + interpolator method was selected.

EXPERIMENTAL SETUP

Electrode ends are observed by reflection in a mirror (**Fig. 1**), thus leaving the camera in a region less exposed to intense axial X-rays. Direct lighting of electrodes does not work, because many caustics build-up in the vacuum window assembly, resulting in over-contrasted images. Rather, a white paper sheet glued to the mirror is used as a diffusive reflector for the optical fibre lighting system, and a small cardboard diaphragm placed against the vacuum window. The camera is a LightWise LW-1.3-S-1394, with a 2048 × 1536 CCD detector, and FireWire link for acquisition. Lead protection is added everywhere it can be.

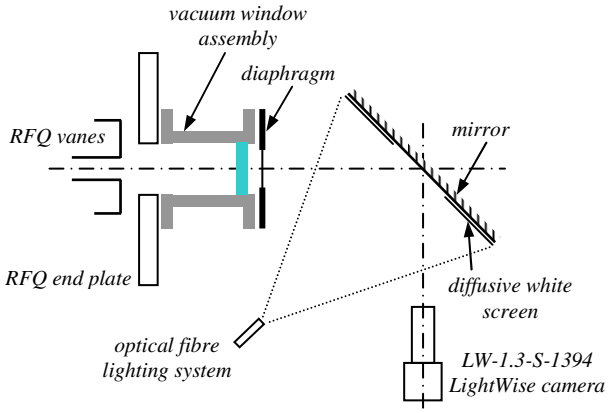

Fig 1. Experimental setup.

DIGITAL PROCESSING

Data flow. Raw RGB images from the camera (without any color or contrast correction that might induce errors

in subsequent processing) are first cropped into four 220 × 220 sub-frames, one per electrode (**Fig. 2**). Each sub-frame is converted into luminance image, using

$$Y = 0.30\ R + 0.59\ G + 0.11\ B.$$

Luminance histogram is computed (64 bins), and contrast is linearly stretched over full range, i.e. lowest intensity maps to 0 and highest intensity maps to 1 (**Fig. 3**). Then a low-pass filter (3×3 Gaussian mask, $\sigma_x = \sigma_Y = 0.6$ pix) is used to smooth out defective pixels. All these operations must be *rigorously* identically performed on all images in a motion detection sequence to prevent any fake motion detection. Sub-frames of "reference" and "current" images are then presented to cross-correlators-interpolators for X and Y motion detection. Data is displayed after compensation of general X and Y drifts, thus only saving relative motions of electrodes. Inter-electrode distance variations are finally computed, and expressed into *RFQ coordinates,* a set of linear combinations directly related to RFQ frequency and voltage perturbations.

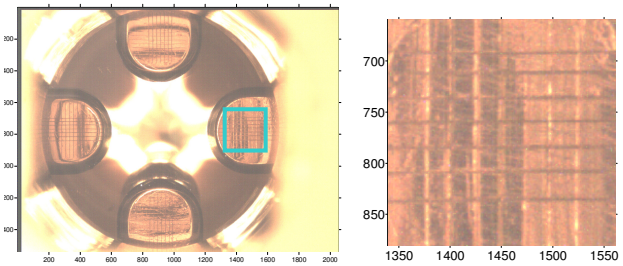

Fig. 2. Left: camera frame, with pixel {1,1} at upper-left and pixel {1536,2048} at bottom-right. Right: 220×220 sub-frame.

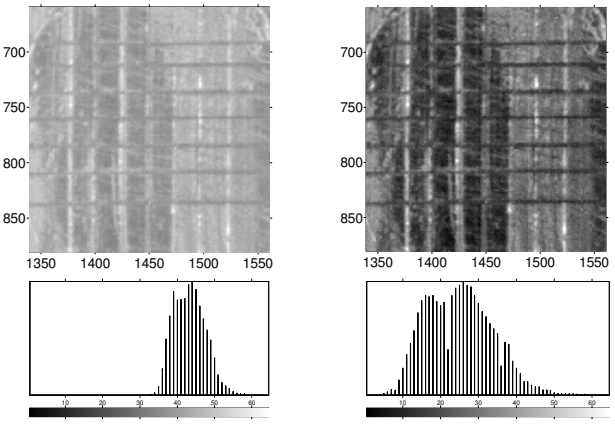

Fig. 3. Contrast enhancement with histogram linear stretching.

Image scaling. Pixel size is derived from grid pattern known metric size (4×4 mm) and observed size in pixel units (averaged over the four electrode sub-frames). With given optics and geometry, pattern size is about 140×140, and pixel size is ~ 28.6 µm.

Normalized cross-correlation. Let A(p,q) and B(p,q) two intensity images in the range [0,1]. Normalized cross-correlation is defined as

$$\chi(i,j) := \sum_{p=1}^{P}\sum_{q=1}^{Q} A'(p+i,q+j).B'(p,q)$$

where A' and B' are normalized zero-mean images

$$\langle A\rangle = \tfrac{1}{PQ}\sum_{p=1}^{P}\sum_{q=1}^{Q} A(p+i,q+j), \quad A' = \frac{A-\langle A\rangle}{\|A-\langle A\rangle\|_2},$$

$$\langle B\rangle = \tfrac{1}{PQ}\sum_{p=1}^{P}\sum_{q=1}^{Q} B(p,q), \quad B' = \frac{B-\langle B\rangle}{\|B-\langle B\rangle\|_2}.$$

Let A be the "current" image, and B the "reference". Then for any integer motion {−u, −v}, the correlation peak appears at χ(u, v) = 1. χ is usually computed over a small mask, to save computation time (here 11×11 typ.). Non-integer motion is dealt with by approximating the correlation peak as

$$\chi(x,y) = a(x-u)^2 + b(y-v)^2 + c(x-u)(y-v) + d$$

$$\equiv g_1 x^2 + g_2 y^2 + g_3 xy + g_4 x + g_5 y + g_6 .$$

The g_i are derived by least-square fit over the correlator output, and a, b, c, d, u, v are obtained by identification. Eigen-values $\lambda_{1,2}$ of the Hessian of χ

$$H_\chi = \begin{vmatrix} g_1 & \frac{1}{2}g_3 \\ \frac{1}{2}g_3 & g_2 \end{vmatrix}$$

are used to estimate full-width half maximums (FWHM) of correlation peak $w_{1,2} = [2/|\lambda_{1,2}|]^{1/2}$, and eigen-vectors give their orientation in image plane.

Partitioned images. Electrode sub-frames are first partitioned in 5×5 blocks, and cross-correlation is performed for the 25 pairs of "reference" and "current" blocks. Inner blocks are 40×40, side blocks are 50×40 or 40×50 and corner blocks are 50×50, thus leaving room for maximum correlation shifts of 10 pix in all directions. Motion estimate is taken to be the mean of all valid correlator-interpolator outputs (i.e. satisfying $\lambda_1 < 0$ and $\lambda_2 < 0$). Note that with proper electrode lighting, correlation peak is always > 0.90, and all blocks are valid. Typical standard deviation over 25 blocks is $\sigma_{X,Y} = 0.1$ to 0.3 pix. Standard deviation of the estimate of the mean is then $\sigma_{X,Y}/\mathrm{sqrt}(25) = 0.02$ to 0.06 pix, i.e. 0.6 to 1.8 µm.

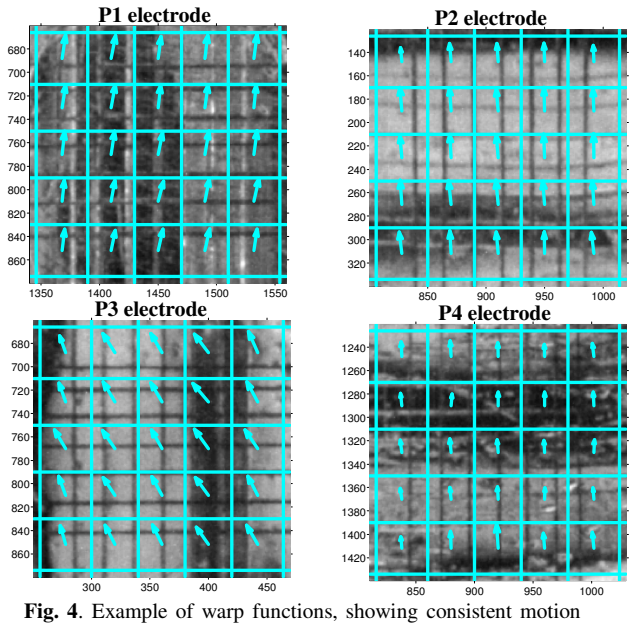

Fig. 4. Example of warp functions, showing consistent motion over partition blocks.

Drift compensation. Detected motions $\{u_n,v_n\}$ are added to coordinates of grating centers in "reference" frame for initial display (**Fig. 5, left**)

$$X_n = X_n^{ref} + u_n,\ \ Y_n = Y_n^{ref} + v_n,\ \ n = 1...4.$$

Erratic aspect comes from uncontrolled movements of optics table relative to RFQ, likely due to poor floor stability, vibrations, and temperature differences. Things look better (**Fig. 5, right**) after subtracting X and Y drifts

$$X_{Drift} = \tfrac{1}{4}(u_1 + u_2 + u_3 + u_4),\quad Y_{Drift} = \tfrac{1}{4}(v_1 + v_2 + v_3 + v_4)$$

from X_n, Y_n.

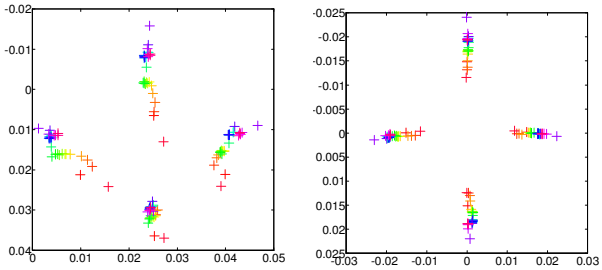

Fig. 5. Motion of grating centers in frame coordinates before (left) and after (right) drift compensation. X and Y in meter units. "Reference" frame data is plotted at true coordinates; subsequent "current" frame motion is amplified 200×.

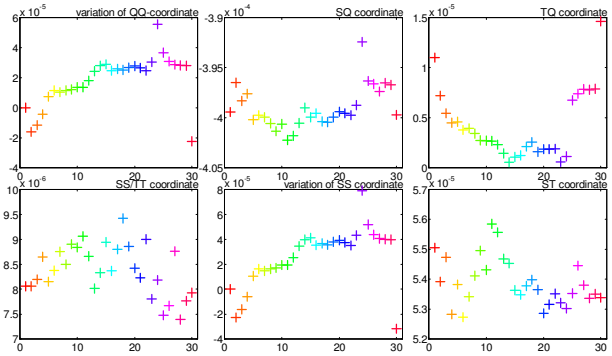

Fig. 6. Motion displayed in RFQ coordinates (meter units), vs. frame index (one frame every 5 minutes). Same color code as in Fig. 5.

RFQ coordinates. Data in **Fig. 5** is presented using 8 parameters per frame; however, relative positions of 4 points in a plane are fully described by only 5, as for instance distances d_{12}, d_{23}, d_{34}, d_{41} and d_{13}. Proposed data reduction uses knowledge of RFQ electrical behavior. Let

$u_{12} = +U_Q+U_S$, $u_{23}=-U_Q+U_T$, $u_{34}=+U_Q-U_S$, $u_{41}=-U_Q-U_T$,

where u_{mn} is voltage difference from electrode #m to electrode #n, U_Q is the quadrupole accelerating voltage, and U_S, U_T the (unwanted) dipole components (note that the quasi-static behavior of RFQ axial region implies $u_{12}+u_{23}+u_{34}+u_{41}=0$). At first order,

$$\Delta U_Q \sim (\Delta C_{12} + \Delta C_{23} + \Delta C_{34} + \Delta C_{41})/4$$

$$\Delta U_S \sim (\Delta C_{12} - \Delta C_{34})/2,\quad \Delta U_S \sim (\Delta C_{41} - \Delta C_{23})/2$$

where ΔC_{mn} is the capacitance variation between electrodes #m and #n. Since capacitances are roughly inversely proportional to electrode separation, we define the following *RFQ coordinates*

$d_{QQ} := (d_{12}+d_{23}+d_{34}+d_{41})/4$, $d_{SSTT} := (d_{12}-d_{23}+d_{34}-d_{41})/4$,

$d_{SQ} := (d_{12}-d_{34})/2$, $d_{SS} := (d_{24}+d_{13})/2$,

$d_{TQ} := (d_{41}-d_{23})/2$, $d_{ST} := (-d_{24}+d_{13})/2$,

any 5 of them fully describing the electrode relative positions (**Fig. 6**). Variations of d_{QQ}, d_{SQ} and d_{TQ} directly relate to RFQ voltage perturbations.

METRICS

Side of etched patterns is measured using manual graphics tools; uncertainty is estimated to be ±2 pix; hence Pixel Size Error is lower than 2/140 = $1.4\ 10^{-2}$. Pole distance variations are obtained by projecting X and Y motions on the line joining pattern centers. Pole-center to pattern-center is never greater than 50 pix, and center-to-center distance is about 750 pix. Hence pole-to-pole axis angular error is $\vartheta \le$ atan 50/750 = 3.8 deg, and Pole-to-Pole Distance Projection Error is smaller than $1-\cos\vartheta = 2.2\ 10^{-3}$. Optical axis has been aligned using vacuum port located on other end of RFQ, hence tilt angle is bounded by $\alpha \le$ atan 0.02/1.00 = 1.14 deg, and Ellipticity Ratio in camera focal plane is smaller than $1-\cos\alpha = 2\ 10^{-4}$. Clearly, overall metrics error could be reduced with high precision pattern etching.

LIGHTS IN THE NIGHT

CCD camera has also captured many bright light-emitting spots, generally showing-up at 20 kW and above (**Fig. 7**). Most of these are located at 45° angle on electrode tips, where electric field is a maximum. They remained quite stable throughout experiments in 2005 and 2006 [1], and are likely related to local surface defects.

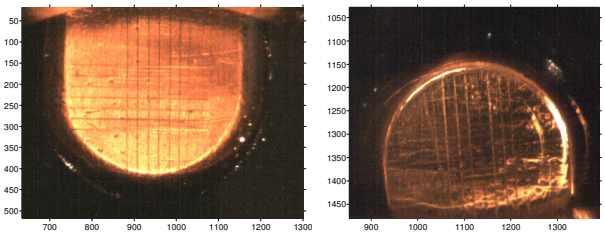

Fig. 7. Light emissions on upper (at left) and lower (at right) vanes, as observed from RFQ output. These are color-enhanced images, with R, G and B contrasts linearly stretched as explained in Fig. 3. Light emission looks white because it saturates the CCD.

REFERENCES

[1] R. Ferdinand & al., *SPIRAL2 RFQ prototype – first results*, EPAC06, MOPCH103 paper.

[2] Y. Keller, A. Averbuch, *Fast motion estimation using bidirectional gradient methods*, IEEE-IP, Vol. 13, No. 8, August 2004.

[3] Y. Cheng & al., *The Mars exploration rovers descent image motion estimation system*, Jet Propulsion Lab, IEEE Computer Society Journal, May/June 2004.

[4] WS Hoge, CF Westin, *Identification of translational displacements between N-dimensional data sets using the high-order SVD and phase correlation*, IEEE-IP, Vol. 14, No. 7, July 2005.

[5] K. Rohr, *Feature extraction*, IEEE Conference on Computer Vision and Pattern Recognition, 2004.